Hybrid reflecting objectives for functional multiphoton microscopy in turbid media

Dejan Vučinić and Thomas M. Bartol, Jr.

Howard Hughes Medical Institute, Computational Neurobiology Laboratory, The Salk Institute for Biological Studies, La Jolla, California 92037

Terrence J. Sejnowski

Howard Hughes Medical Institute, Computational Neurobiology Laboratory, The Salk Institute for Biological Studies, La Jolla, California 92037, and Division of Biological Sciences, University of California, San Diego, La Jolla, California 92093

Received March 20, 2006; revised May 23, 2006; accepted May 29, 2006; posted June 2, 2006 (Doc. ID 69133); published July 25, 2006

Most multiphoton imaging of biological specimens is performed using microscope objectives optimized for high image quality under wide-field illumination. We present a class of objectives designed *de novo* without regard for these traditional constraints, driven exclusively by the needs of fast multiphoton imaging in turbid media: the delivery of femtosecond pulses without dispersion and the efficient collection of fluorescence. We model the performance of one such design optimized for a typical brain-imaging setup and show that it can greatly outperform objectives commonly used for this task. © 2006 Optical Society of America

OCIS codes: 170.2520, 170.7050.

The application of multiphoton excitation[1,2] to biological imaging has greatly extended the usefulness of microscopic techniques as tools for the study of neuronal morphology and activity. One of the most important advantages of multiphoton excitation over other methods for functional imaging of neuronal activity is the confinement of excitation to a very small, micrometer-sized, region around the focal spot. Many fluorescent dyes have been developed that report various aspects of neuronal activity through a change in their fluorescent cross section. The hard physical limit on how small a change in the reported quantity can be measured in a given amount of time is the shot noise—the noise resulting from the probabilistic nature of absorption and emission of individual photons. If wide-field illumination is used to excite fluorescent molecules in bulk-loaded neuronal tissue, the collateral shot noise from all the fluorescence photons emitted above and below the plane of focus can obscure any signal coming from the focal plane and so thwart the measurement of faint or fast changes. Confocal scanning microscopy suffers the same limitation, since the pinhole cannot distinguish between fluorescence photons coming from the focus and background photons whose final trajectories upon exit from tissue intersect with the location of the focal spot. Here multiphoton excitation comes to the rescue by not exciting in the first place any locations away from the focus: the optical sectioning inherent in nonlinear excitation means that nearly every fluorescence photon that can be collected must have originated at the focus regardless of scattering. This permits more efficient detection of fluorescence than is possible with confocal techniques.

The small size of the volume excited in multiphoton and confocal techniques severely limits the number of fluorescent molecules that can be excited in a given amount of time, making every emitted photon precious. In epifluorescence imaging, a large fraction of these emitted photons is typically lost right at the outset. For instance, the ubiquitous 40×0.8 NA water-immersion objectives commonly used for two-photon imaging of neurons *in vivo* have a geometrical acceptance of ~10% before any losses inside the objective and the microscope are taken into account. This inefficiency alone reduces the shot noise-limited signal-to-noise ratio by more than a factor of 3 from its physical limit. When imaging in a highly turbid but weakly absorbing medium, such as cortical gray matter where the scattering length is a few orders of magnitude shorter than the absorption length, this problem can be exacerbated by the high magnification of the objective, making it more likely that scattered fluorescence photons that do get collected by the objective ultimately miss the detector.[3–6] In addition to these detection inefficiencies, most widely used objectives are corrected and coated for a wavelength range shorter than that of excitation light typically used in biological multiphoton imaging. Any residual aberrations and losses at longer excitation wavelengths limit their utility in functional imaging of living tissue in two important ways: by reducing the available imaging depth for a given laser power and by increasing the rate of heating of tissue, possibly affecting the physiological processes under observation, if fluorescence intensity must be kept constant. To reach the physical limits of the ability to measure fast and small changes in neuronal membrane voltage we set out to design a class of microscope objectives that minimize these problems.

The concept of a hybrid objective is illustrated in Fig. 1. Excitation pulses are delivered through a refracting or reflecting image-forming pathway of moderate numerical aperture (NA). Emitted fluorescence is also collected by a nonimaging mirror configured to extend to the maximal aperture permitted by the geometry of the specimen. The image-forming pathway can be constructed using a wide variety of existing

0146-9592/06/162447-3/$15.00

objective designs, e.g., by simply adding a reflective shroud around the modern designs used in patch clamping[7,8] as illustrated in Fig. 1(b). The use of a nonimaging pathway for fluorescence collection relaxes a number of constraints on the design of the imaging pathway. For example, a small portion of the nonimaging mirror can easily be cut out to allow access to tissue with electrodes with no adverse effect on image quality and with minimal loss of fluorescence collection efficiency [Fig. 1(c)], an approach not practical with traditional refracting objectives of very high NA.

The complexity of combining the imaging and nonimaging optical paths and building a mechanically robust objective with a refracting imaging pathway would likely necessitate the construction of a custom microscope. We therefore decided to optimize an all-reflecting hybrid (HR) design constrained by the dimensions of a realistic brain-imaging setup—a common Nikon Eclipse E600FN upright microscope. The distance between the specimen surface and the objective mount was restricted to 65 mm. The working distance was set to 1 mm, the practical scattering-induced depth limit for two-photon excitation.[9] The image-forming portion was constructed out of two aspheric mirrors, M1 and M2, arranged in a Cassegrain configuration,[10,11] and its NA set to 0.65 in air (up to approximately 0.86 in a water-immersion configuration) to achieve a satisfactory resolution of multiphoton excitation along the z axis. The design was optimized for use with an acousto-optic deflector with a time–bandwidth product of 300 and a full deflection range of 2.8°, so first the location and the radius of curvature (ROC) of the aspheric mirror M1 were chosen to achieve the desired magnification ($\sim 30\times$) to cover the field of view of approximately 200 μm. The aspheric shapes of mirrors M1 and M2 were then optimized by using ZEMAX software (ZEMAX Development Corporation, Bellevue, Washington) to minimize aberrations within this field of view. The optimal solution, detailed in Table 1, has the optical path difference well below $\lambda/4$ throughout the entire field of view at near-infrared wavelengths. Since only reflecting surfaces are used, this objective introduces negligible temporal dispersion into the propagation of femtosecond pulses. The dominant aberrations limiting the performance of this design are spatial, namely, the spherical aberration and the astigmatism that prevent the focusing of femtosecond pulses into a diffraction-limited volume. To estimate their summed effect, in Fig. 2 we plot the profile of encircled energy at three regions within the field of view. The design is nearly diffraction limited throughout most of the field of view, with only a slight worsening in the corners.

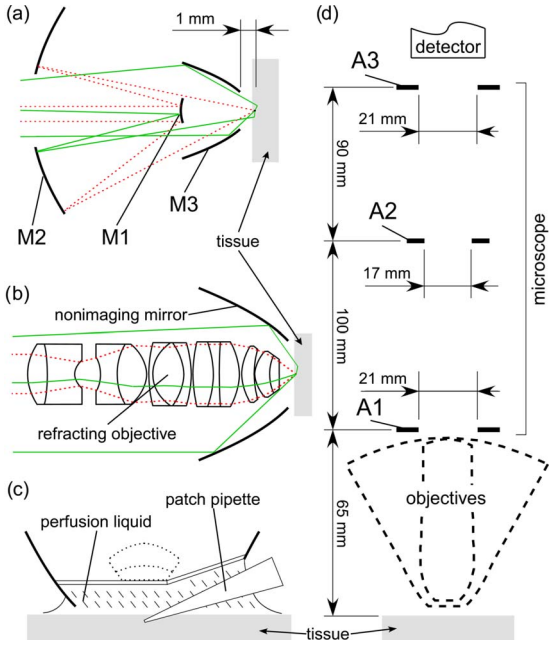

Fig. 1. (Color online) (a), (b) Hybrid objectives for multiphoton imaging. (a) All-reflecting design (HR) consisting of image-forming mirrors M1 and M2 arranged in a Cassegrain configuration, and a nonimaging mirror M3 that increases the efficiency of epifluorescence collection. Dotted red and solid green rays illustrate the paths of excitation pulses and fluorescence photons, respectively. (b) Slightly higher collection efficiencies are achievable in principle by using a refractive imaging portion without a central obstruction. (c) Relaxed optical requirements for the nonimaging mirror allow part of it to be removed to permit access to tissue with electrodes while incurring a minimal loss of collection efficiency. (d) Virtual test setup for comparison of epifluorescence collection efficiency. Emitted photons were scattered in tissue and propagated through the objectives and three apertures (A1, objective mount; A2, filter cube; A3, detector mount) placed to mimic the arrangement in the Nikon Eclipse E600FN upright microscope.

To evaluate the efficiency of epifluorescence collection, we performed a Monte Carlo simulation of scattering in a semi-infinite turbid slab[4] using ZEMAX software. We compared the performance of our HR design with that of the models of three modern water-immersion objectives with long working distances: Olympus 40×0.8 NA and 60×0.95 NA,[7] and Nikon 100×1.1 NA.[8] All the objectives were evaluated within the same microscope geometry, shown in Fig. 1(d). The collected fluorescence was required to pass through the three apertures inside the microscope to be considered detected. Figure 3 shows that the HR design has much higher epifluorescence collection efficiency at all imaging depths, as expected from the large geometric acceptance of the nonimaging pathway. The benefits of higher NA of the $100\times$

Table 1. Parameters (mm) of the HR Objective Design Optimized for No Index Mismatch

Mirror	ROC	Conic	$\times r^4$	$\times r^6$	$\times r^8$	$\times r^{10}$	d	$r_{\min}$	$r_{\max}$
M1	6.5	0.876	-2.857×10^{-4}	-7.594×10^{-6}	-2.241×10^{-7}	-1.442×10^{-8}	−45		2.9
M2	54.648	1.3×10^{-4}	-1.828×10^{-9}	-3.967×10^{-13}	1.678×10^{-17}	-6.175×10^{-20}	66.0483	10.5	42
M3	−5.988	−0.93					−3.0483	6.9	13.5

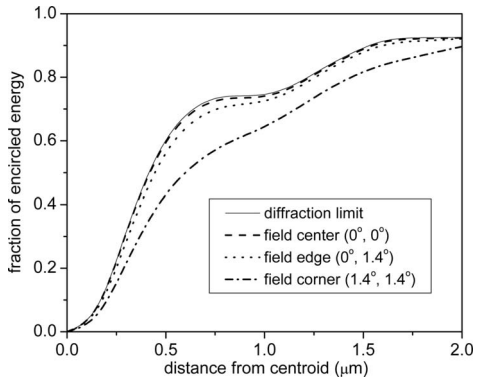

Fig. 2. Multiphoton imaging resolution of the HR design detailed in Table 1 is limited by the sum of all spatial aberrations of excitation pulses delivered through the imaging pathway, plotted here as the fraction of encircled energy delivered within a given distance from the centroid of the focal spot. A slight worsening of the resolution is evident only in the corners of the 200 μm field of view.

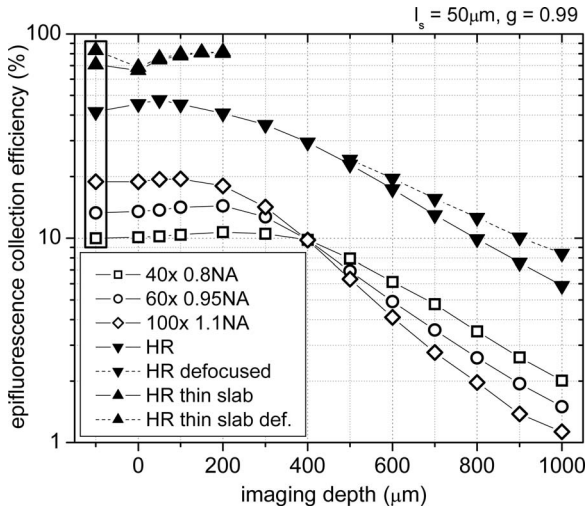

Fig. 3. Comparison of epifluorescence collection efficiency as a function of imaging depth in a semi-infinite turbid slab. HR design with the parameters in Table 1. Dashed curves indicate that the configuration of the HR objective was modified by defocusing the nonimaging reflector to maximize the collection efficiency. The outlined values at negative imaging depths refer to a nonscattering sample. The "thin slab" configuration refers to a 200 μm thick slab placed in a recording chamber with a reflecting bottom. The crossing at 400 μm is an artifact of objective selection.

and 60× objectives are lost at greater depths, because the likelihood of multiply scattered photons reaching the detector decreases as the magnification of the objective increases. The simulations of the refracting objectives did not take into account internal reflections or the losses at any apertures placed internally to improve off-axis image quality. Tissue surface was modeled as smooth and nonreflective. The losses at the central obstruction of the HR design are approximately 0.5%; for comparison, losses of similar magnitude would result from increasing the working distance by only 80 μm.

Scattered photons appear to come from a location different than their true origin: in a highly turbid semi-infinite slab the apparent source of fluorescence photons is a diffuse region extending about one scattering length below the surface of the medium with a radial extent linearly dependent on the imaging depth.[4] This suggests the possibility that the collection efficiency of the HR objective could be improved even further by displacing the nonimaging pathway relative to the focus of the imaging pathway. Similarly, a displacement in the opposite direction would be beneficial in the case where a thin turbid slab is placed in a recording chamber with a reflecting bottom, a model pertinent to the imaging of behaving *Caenorhabditis elegans* for instance. The magnitudes of these improvements are indicated by the dashed curves in Fig. 3.

In conclusion, we introduced a class of hybrid microscope objectives with separate imaging and nonimaging portions. Such objectives are better suited to functional multiphoton imaging in turbid media than the traditional refracting objectives. We optimized one such all-reflecting design given the constraints of a realistic brain-imaging situation. We achieved nearly diffraction-limited performance of the imaging portion throughout a 200 μm field of view with a relatively high NA and negligible temporal dispersion of femtosecond pulses. More importantly, we demonstrated a practical way to achieve a twofold to fourfold improvement in epifluorescence collection efficiency over traditional objective designs while maintaining the working distance required for deep-tissue imaging. Wider commercial availability of hybrid objectives such as the ones described here would enable physiological recordings of longer durations with less tissue damage, as well as the recording of faster and smaller fluorescence changes.

We thank Sanja Zlatanović for ZEMAX, and Richard Jacobs for help with lathework. D. Vučinić's email address is dejan@salk.edu.

References

1. W. Denk, J. H. Strickler, and W. W. Webb, Science **248**, 73 (1990).
2. F. Helmchen and W. Denk, Nat. Methods **2**, 932 (2005).
3. M. Oheim, E. Beaurepaire, E. Chaigneau, J. Mertz, and S. Charpak, J. Neurosci. Methods **111**, 29 (2001).
4. E. Beaurepaire and J. Mertz, Appl. Opt. **41**, 5376 (2002).
5. A. Taddeucci, F. Martelli, M. Barilli, M. Ferrari, and G. Zaccanti, J. Biomed. Opt. **1**, 117 (1996).
6. A. N. Yaroslavsky, P. C. Schulze, I. V. Yaroslavsky, R. Schober, F. Ulrich, and H.-J. Schwarzmaier, Phys. Med. Biol. **47**, 2059 (2002).
7. A. Katsuyuki, Olympus Optical Company, Ltd., Japanese patent 8-292374 (November 5, 1996).
8. K. Watanabe, Nikon Corporation, Japanese patent 2001-319653 (2001), U.S. patent 6,700,710 (March 24, 2004).
9. P. Theer, M. T. Hasan, and W. Denk, Opt. Lett. **28**, 1022 (2003).
10. S. Kashima, Olympus Optical Company, Ltd., Japanese patents 3-050518 (March 5, 1991), 3-050519 (March 5, 1991), 3-058009 (March 13, 1991), 3-058010 (March 13, 1991), U.S. patents 5,144,496 (September 1, 1992), 5,253,117 (October 12, 1993), 5,291,340 (March 1, 1994).
11. H. Hiroshi, Mitsubishi Electric Corporation, Japanese patent 59-077403 (May 2, 1984).